Publ. Astron. Soc. Japan, **41**, 391-403 (1989)

All Sky Monitor on Board the Ginga Satellite and Its Performance

Hiroshi TSUNEMI, Shunji KITAMOTO, Makoto MANABE,*
Shigenori MIYAMOTO, and Koujun YAMASHITA

Department of Physics, Faculty of Science, Osaka University, 1-1, Machikaneyama-cho, Toyonaka, Osaka 560

and

Michio NAKAGAWA

Department of Physics, Faculty of Science, Osaka City University, 3-138, Sugimoto 3-chome, Sumiyoshi-ku, Osaka 558

(Received 1988 September 2; accepted 1988 December 11)

Abstract

We present here a description of the X-ray All Sky Monitor (ASM) on board the satellite Ginga. The ASM consists of two identical gas proportional counters operating in the energy range between 1 and 20 keV. The instrument is subtended by six different collimators with a field of view of roughly $1° \times 45°$. The collimators are arranged symmetrically in six different slant-angle positions: $\pm 8°$, $\pm 24°$, $\pm 42°$, respectively, about the Z-axis of the spacecraft. Each has an effective area of about 70 cm^2. These collimators are especially effective for resolving sources in densely packed regions such as the Galactic center. The instrument has functioned well since the February 1987 launch. It is the only wide-field-of-view X-ray monitor operating this decade. The ASM is uniquely capable of achieving two important objectives: (1) it serves as a real-time alarm for new transient phenomena, and provides fast-response data for studying the temporal and spectral behavior of sources. A good example of this is the discovery of the new nova GS 2000+25. (2) It provides a sensitive, long-term historical record of X-ray sources which can be made available for archival investigation (e.g. Cir X-1). We discuss the capabilities and performance of the instrument, and present sample illustrations of scientific data from the ASM.

Key words: Instruments; X-rays; X-ray sources.

1. Introduction

The third Japanese X-ray astronomy satellite, named Ginga (Makino and the ASTRO-C team 1987), was successfully launched on February 5, 1987 from Kagoshima

* Present address: Chuo High School, Kagawa-cho, Kagawa-gun, Kagawa 711.

Space Center. The primary instrument on board is an array of Large Area gas proportional Counters (LAC) with $\sim 4000\,\mathrm{cm}^2$ total effective area, and a field of view of $0.^{\circ}7 \times 1.^{\circ}5$. Details of LAC are described by Turner et al. (1989). A second instrument to observe X-rays from celestial objects is the All Sky Monitor (ASM). The ASM complements the LAC experiment, because it has a large field of view ($1^{\circ} \times 45^{\circ}$) and covers about 70% of the sky when the satellite rotates around its Z-axis.

An X-ray all sky monitor system can provide two independent capabilities: a real-time alarm for transient phenomena and a historical record for archival investigation. Vela 5B XC (Priedhorsky et al. 1983) which functioned between May 1969 and June 1979 was the first such experiment. However, the sensitivity of the instrument was somewhat limited by the high background, and it therefore achieved the somewhat high detection limit of about 250 UFU (Uhuru Flux Unit) in one day of observation. The next X-ray all sky monitor system was the Ariel V ASM which functioned for six years between 1974 and 1980. Ariel V ASM consisted of two one-dimensional pin-hole camera systems with an effective opening area of $1\,\mathrm{cm}^2$, and achieved a sensitivity limit of about 100 UFU for one-day's observation (Holt 1976). However, because of the limited telemetry rate, the instrument had serious source confusion problems, especially for sources near the galactic center. There were several other large scanning experiments which were later used to survey the sky. However, because of their narrow fields of view, these experiments only provided irregular or intermittent monitoring of cosmic sources. For example, HEAO-1 also conducted an all-sky survey in which the spin axis was pointed to the solar direction. While the sky regions near the ecliptic poles was continuously monitored, regions near the ecliptic equator were sampled only twice a year.

As a sensitive, wide-field X-ray monitor the Ginga ASM experiment has better overall capabilities than those of the previous experiments. The instrument has a better detection sensitivity, a wider coverage of the sky, and greater spatial resolution for minimizing source confusion. In section 2, we describe the detailed characteristics of the instrument. Examples of observational results are presented in section 3.

2. Instrumentation

2.1. X-Ray Detectors

The ASM consists of two identical gas proportional counters of which the gas content comprises xenon at a partial pressure of 736 mmHg and CO_2 at a partial pressure of 25 mmHg when operating at STP. The effective interaction depth of the instrument is 28 mm. The two counters are named Y1 and Y2, respectively. In figure 1, we show a cross sectional view of one of the counters. The wall of the counter is made of magnesium alloy. Each counter is also shielded at the sides and at the rear with lead foil 0.3 mm thick for the purpose of eliminating nonaperture background photons. The front entrance window consists of beryllium 50 μm thick.

There are three chambers in each of the two detectors. They are named W1, W2, and W3. The three chambers operate independently, and provide each other with mutual anticoincidence shielding. Small holes were made through the partition walls for

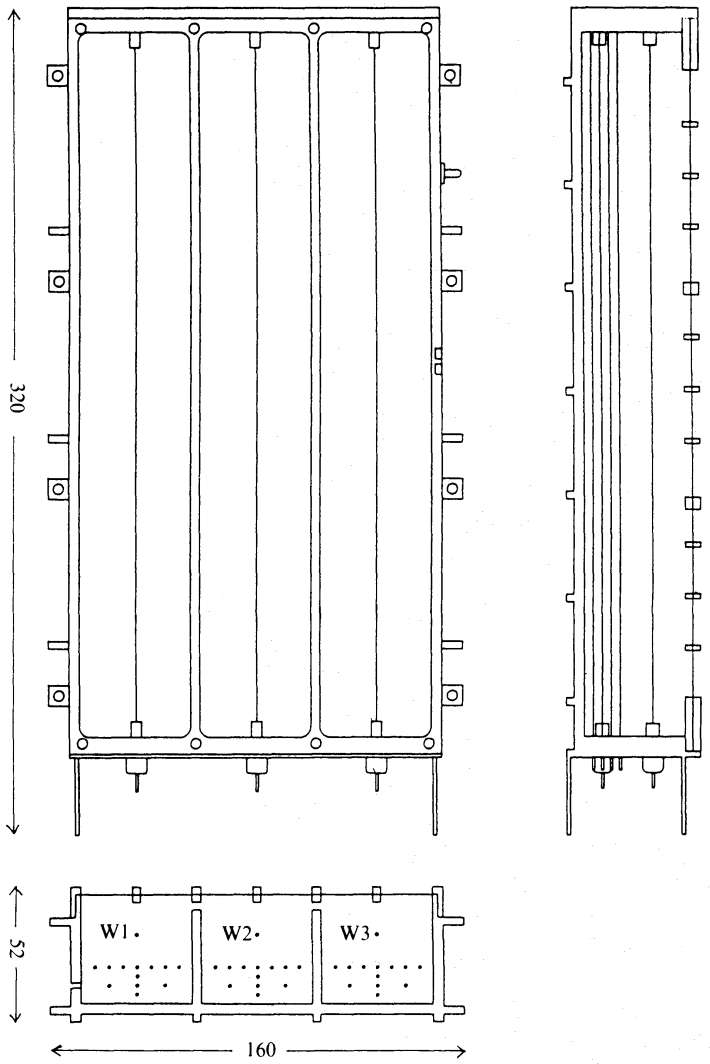

Fig. 1. The outline of the ASM counter and its cross section. The wall of the counter is made of magnesium alloy and the entrance widow is beryllium with a thickness of 50 μm. It is shielded at the sides and at the rear with 0.3-mm thick lead foil for the purpose of eliminating the nonaperture background photons.

equalizing the gas pressure and composition between chambers. A single 35-μm diameter anode wire was placed in the center of each chamber. Valid X-ray events measured by one chamber are defined as those which are not accompanied by any coincidence events in the other chambers. There are two additional 50-μm diameter wires placed in the bottom section of each chamber. They serve as veto-gates for increasing the rejection efficiency of non-X-ray events. The diameter of these front and rear wires was selected to allow equal gas gain throughout the chamber. Signals from six rear anode wires are electronically summed and provide a single veto anticoincidence pulse for non-X-ray events. One of these rear anode wires is also exposed continuously to an on board ^{55}Fe radio-active source which is used primarily to monitor the condition of the detector. In summary, ASM has a total of six chambers with two gas proportional counters. They are identified as Y1–W1, Y1–W2, Y1–W3. Y2–W1,

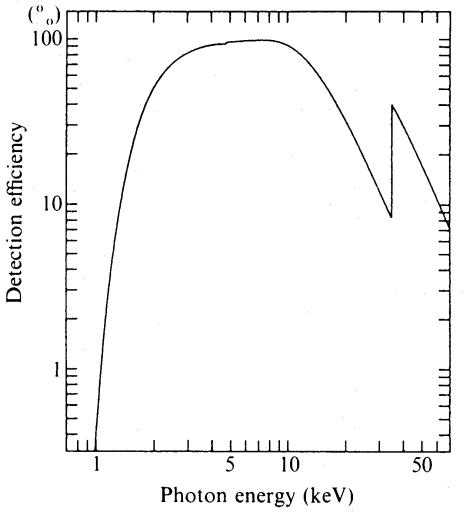

Fig. 2. The detection efficiency is shown for the ASM W1, W2, and W3 against the incident X-ray energy including the absorption by the window. The normal condition of the ASM covers the enery range between 1 and 20 keV.

Y2–W2, and Y2–W3, respectively.

Figure 2 shows the detection efficiency, including the absorption effect of the front beryllium window, for incident X-rays measured by the front wire (W1, W2, W3) of each chamber. The probability of X-rays below 20 keV penetrating through the side and rear walls is less than 0.1%.

Each counter is equipped with a high voltage supply. Normally the voltage is kept high when the data recorder is in operation, except during passage through high background regions such as the radiation belts. We set the energy range between 1 and 20 keV in the normal observation mode.

2.2. *Collimator*

The Ginga satellite can be rotated about the Z-axis with an angular velocity up to about $20^\circ\,\mathrm{min}^{-1}$ by controlling the momentum wheel. However, the Z-axis can only be moved at a maximum rate of several degrees per hour, since we employ the magnetic torquer to move it. The LAC is oriented towards the +Y-axis of the satellite coordinate system, while both the ASM counters Y1 and Y2 are oriented towards the −Y-axis. The normal of the solar panels is oriented to the −Z-axis. The satellite is maneuvered to keep the position of the Sun to be within 45° of the $-Z$-axis in order to comply with power consumption restrictions. Therefore, the field of view of the ASM was designed to exclude the region less than 45° from the $-Z$-axis in order that strong solar X-rays should not damage the proportional counters.

Each chamber of the counter is equipped with a fan beam collimator made of stainless steel. The beam size is limited to roughly $1^\circ \times 45^\circ$ (FWHM). For photons with energy below 20 keV, the penetration probability from outside the beam size is less than 1%. As a result of these collimators, each of the ASM chambers has a maximum effective area of about $70\,\mathrm{cm}^2$.

These fan beams slant at different angles with respect to the Z-axis. Figure 3 shows the projection of the field of view on the satellite coordinates (bottom to bottom).

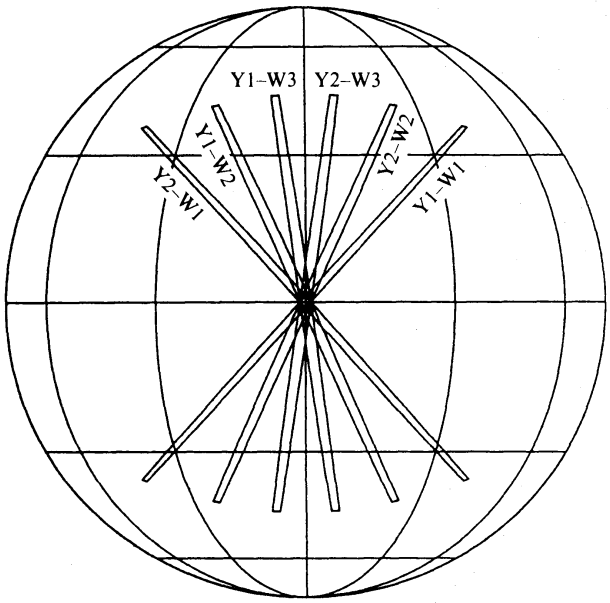

Fig. 3. The projection of the field of view of the ASM (bottom to bottom) in satellite coordinates. The cross point of the six fields of view is in the opposite direction to the LAC field of view. The effective area of each window is about 70 cm^2 through the collimator.

The slanting angles are +42° (Y1–W1), +24° (Y2–W2), +8° (Y2–W3), −8° (Y1–W3), −24° (Y1–W2), and −42° (Y2–W1), respectively. These six fields of view cross roughly at the −Y-axis. When the satellite rotates around its Z-axis, the ASM scans the part of the sky shown in figure 3. When the source is at higher elevation angles, the transit time over the six collimating windows is longer. We can calculate the source position in satellite coordinates from the acquisition angles of the six windows.

2.3. Data Acquisition Modes

There are three main telemetry modes employed in the Ginga operations: the LAC mode, the attitude control system (ACS) mode, and the ASM mode. Data from the ASM consist of two kinds: pulse height data and pulse count (PC) data. Pulse height data are obtained only in ASM mode, while PC data are obtained in all three data modes. In ASM mode, there are two submodes: PHA and TIME mode. PHA data consist of information from 16 pulse height channels for each chamber. PHA data normally covers the energy range between 1 and 20 keV. The width of each channel varies semilogarithmically; the width of channels 1–8 is half that of channels 9–12 and is a quarter that of channels 13–16. The data in the TIME mode consist of 2 channels, each of which corresponds to the sum of channels 1–8 and channels 9–16 in the PHA mode.

There are three kinds of bit rate for data accumulation, high, medium, and low. The full data set in the PHA mode is obtained every 1/16 s, 1/2 s, and 2 s, depending on the bit rate. The data rate in the TIME mode is 8 times faster than that in the PHA mode, there being more timing information at the expense of pulse-height information. The highest time resolution of the ASM is 1/128 s.

PC data for each chamber give only the total number of events. This is available

even when the satellite is not in the ASM mode. PHA data are generally affected by the dead time, arising from the analog-to-digital converter, when the source intensity is stronger than a few times that of the Crab Nebula. PC data are not affected by such a condition. PC data are obtained every 1/16 s, 1/2 s, and 2 s, depending on the bit rate.

2.4. *Calibration*

The energy spectrum of the ^{55}Fe calibration source, measured by the rear veto counter, is available in all data modes. Therefore, we can continuously monitor the gain and obtain the absolute energy scale. The Crab Nebula was observed for several minutes in the pointing mode on March 6, 1987 in order to verify the performance of the counter. This provides an accurate inflight calibration of the response and efficiency of the counters. The Crab Nebula data were analyzed by using a single power-law spectrum with an index α, including the column density N_H due to interstellar absorption. We obtained the power-law photon index α of 2.03 ± 0.04 and $\log N_H$ of 21.69 ± 0.13 (90% confidence level) which are consistent with previous observations (Toor and Seward 1974; Koyama et al. 1984). The minimum χ^2 is 28.6 for 13 degrees of freedom. This value formally excludes the single power-law hypothesis. However, if we take into account the systematic error of about 0.5%, mainly due to the uncertainties in the width of each channel, the reduced χ^2 becomes unity. In figure 4, we show the X-ray spectrum of the Crab Nebula as well as thet best-fit model spectrum described above. During a typical scanning-mode observation by the ASM, most sources are

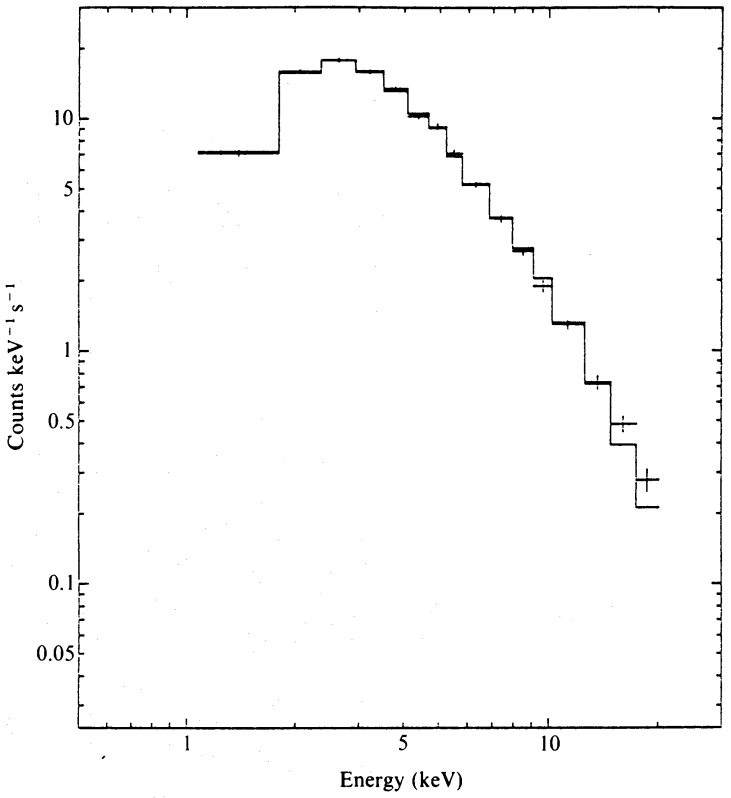

Fig. 4. The energy spectrum of the Crab Nebula with the ASM. Superposed upon the data points is the best fit power law spectrum including the interstellar absorption feature.

observed for several seconds instead of several minutes or more in the pointing mode. Therefore, the systematic errors in scanning mode are usually negligible compared with the statistical errors.

From the slow scan of the Crab Nebula we determined the angular response of the short side of the fan beam collimator to be about 1° (FWHM). This is consistent with the design parameters. The calibration of long side of the fan bean collimator requires several scans as the position angle of the Crab Nebula changes according to the satellite attitude. With this calibration, we can determine the source position with an accuracy of better than 0°.5.

2.5. *Observation and Analysis Methods*

When the satellite is rotated about its Z-axis for 20 min for the purpose of covering a wide sky region with the ASM, this operation is called "slew 360." Such an operation is usually performed once a day during which Ginga is in the ASM mode with the medium bit rate. Under these conditions, we can obtain the 16 channel pulse height data with an angular interval of 0°.15 for each chamber. All the accessible region cannot be covered with a single slew 360 due to Earth occultation. Therefore, we need a few days to cover the whole accessible region of the sky.

We routinely compare the observed data with results obtained from a simulation. The simulation is calculated by using known sources whose positions are fixed, and whose intensities are determined from model fits as free parameters. In this way, we can calculate the intensities of known sources. The residuals determined from the differences of the data and the best-fit simulation should be flat within the statistical uncertainties when no new source appears in the field of view. If a new source appears, we discover it from the residuals.

2.6. *"Slew 360" Observation and the Detection Limit*

Figure 5 shows an example of the six data sets obtained with the ASM during a 20-min observation on April 7, 1987. They are shown from top to bottom according to the slant angle. These data are obtained from the first single slew 360 observation along the galactic plane. The galactic longitude shown in the horizontal axis corresponds to a scanning rate of $18° \text{ min}^{-1}$. In each figure, we draw two data sets; one for energies 1–20 keV and the other for 6–20 keV. The intensity of the Crab Nebula in each graph is about 190 counts s^{-1} (1–20 keV) and about 45 counts s^{-1} (6–20 keV), respectively. Each bin corresponds to 1 s, while the time resolution of data acquisition is 0.5 s.

The background levels shown in figure 5 are representations of those normally measured by the ASM. The average rate in the 1–20-keV range in each chamber is about 18 counts s^{-1}. A half of this value is due to the diffuse X-ray component. When the ASM scans over the Earth, the count rate occasionally increases due to solar X-rays scattered by the upper atmosphere. However, since the scattered solar X-rays are extremely soft, the effect is small above few keV. The remaining half of the background level is primarily due to those high-energy particles which are not rejected by anticoincidence.

Figure 5 shows that many sources can be seen by the ASM. The source position

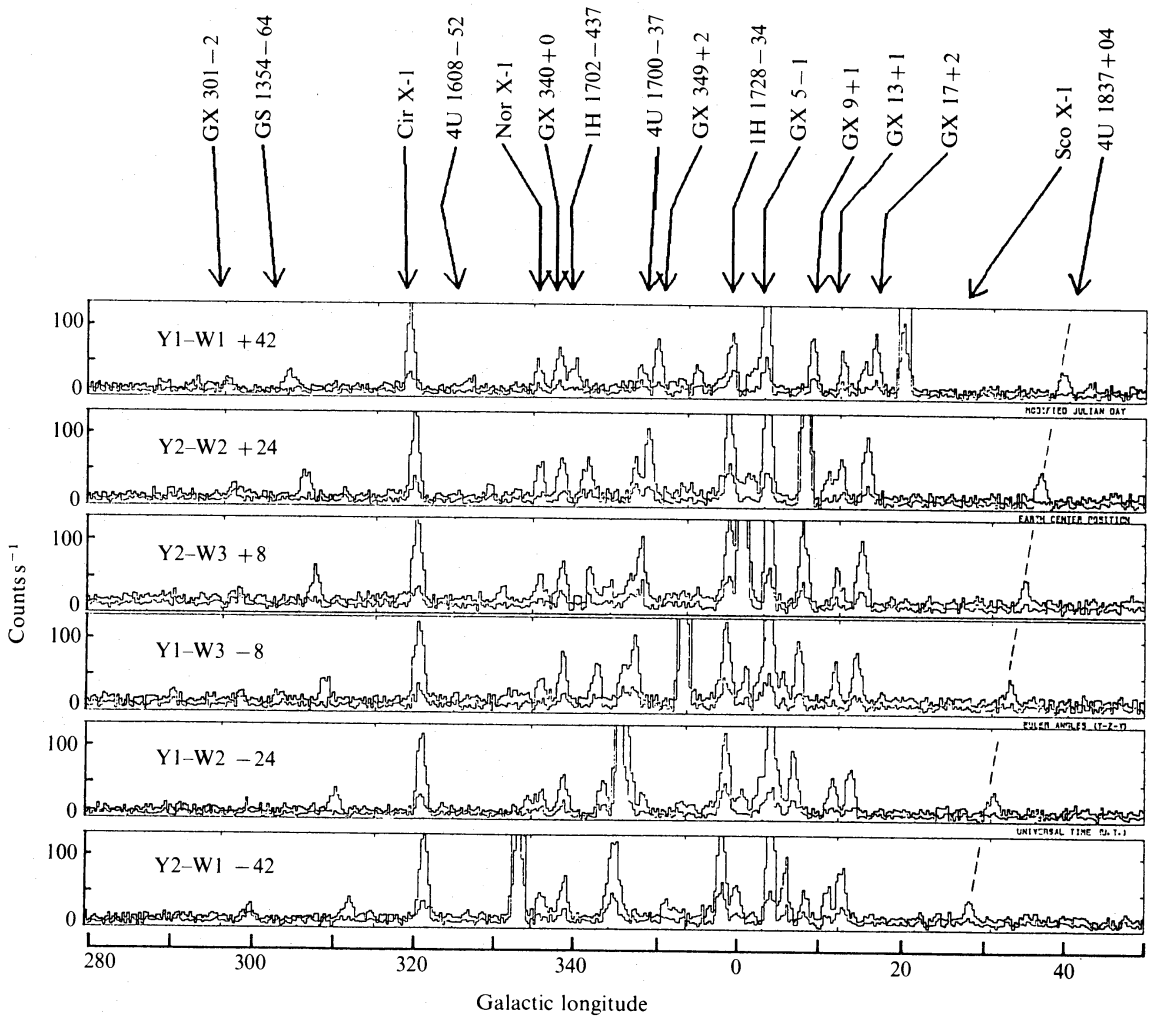

Fig. 5. An example of the six data sets obtained with the ASM during a 20-min observation on April 7, 1987. They are shown from top to bottom according to the slant angles. The galactic longitude shown in the horizontal axis is scanned with speed of $18° \text{ min}^{-1}$. In each figure, we draw two data sets: one for energy 1–20 keV and the other 6–20 keV. The intensity of the Crab Nebula is about 190 counts s^{-1} (1–20 keV) and 45 counts s^{-1} (6–20 keV). Each bin corresponds to 1 s, while the time resolution of data acquisition is 0.5 s.

can be determined by using the differences of the source arrival times in the six chambers. The sources near the satellite equator are seen at almost the same acquisition times, while those at high elevation angles from the equator are seen at different acquisition times. Since the six sets of fan beam collimators are arranged symmetrically, the peak positions of 4U 1837+04, as an example, line up in the way shown by the dashed lines. The source was 6°.3 above the satellite equator. The slant angle of the dashed line corresponds to the elevation angle of the source. Other prominent sources are identified with arrows in the figure. It is important to note that several sources can be merged into a single peak in some windows, while resolved into separate peaks in other windows.

The detection limit of the ASM depends not only on the background condition

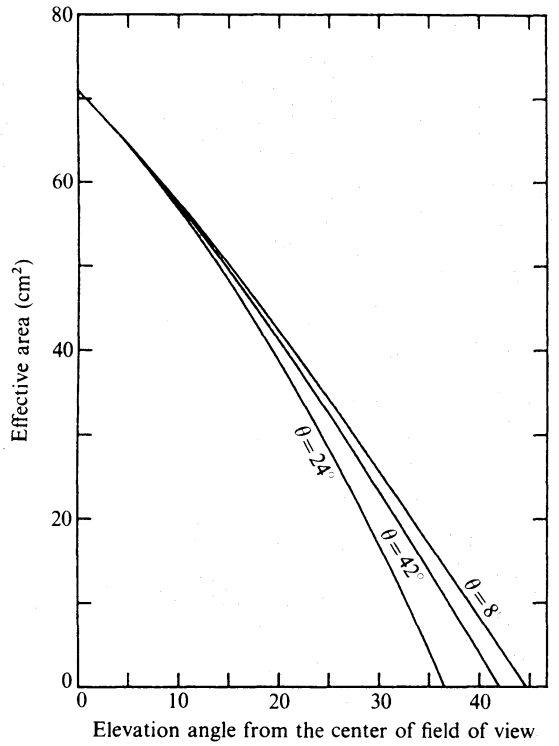

Fig. 6. The effective area of each window of the ASM against the elevation angle of the source. In this figure, we assumed the maximum effective area to be 72 cm^2, although there is a small difference from this value in each window.

but also on the angular distance of the source from the satellite equator. Figure 6 shows the effective area of each window against the elevation angle from the satellite equator. Under normal conditions during the scanning observation shown in figure 5, the detection limit at the 5σ level is less than 50 mCrab for a source in the satellite equator. However, when the source is at an elevation of 30° away from the equator, the detection limit increases up to 200 mCrab. This value further increases with source confusion but decreases at slower scanning speed.

3. Observation Results

3.1. Real Time Alarm for Transient Phenomena

ASM scanning observations in slew 360 are made routinely on the average of once per day. So far, we have detected several X-ray transients (e.g. F. Makino and Ginga team, *IAU Circular* No. 4342, 1987 and No. 4588, 1988): for example, an X-ray outburst from 4U 0115+63 and the X-ray novae GS 1354−64, GS 2000+25. Our observation of these sources gave positions accurate to better than 0°.2. The source 4U 0115+63 is one of the well known X-ray transient pulsars which was observed even during the early test-phase of the satellite program in 1987 (Tsunemi and Kitamoto 1988). Our data showed that the X-ray outburst followed the optical outburst observed by H. Mendelson and T. Mazeh (*IAU Circular* No. 4350, 1987).

The X-ray nova GS 1354−64 showed a soft spectrum in contrast to that of

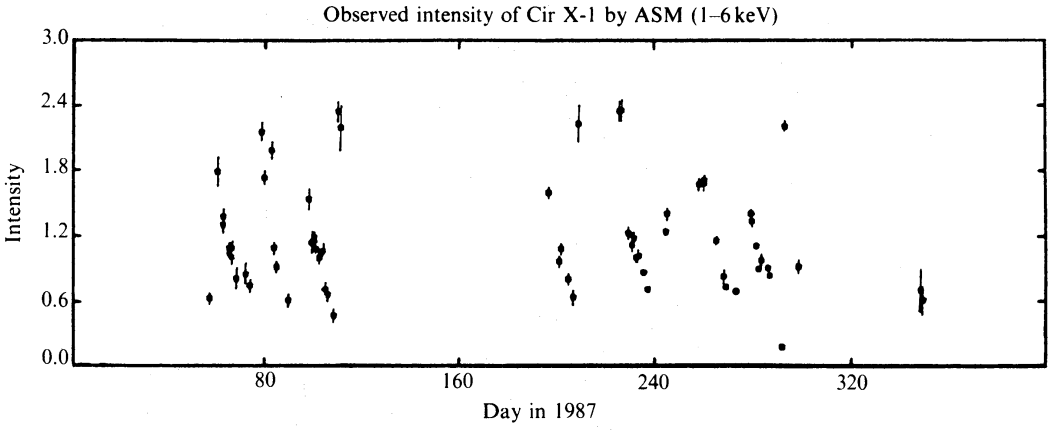

Fig. 7. The light curve of Cir X-1 between February and December, 1987 is shown in the energy range of 1–6 keV. On the vertical scale the value 1.8 corresponds to the intensity of the Crab Nebula. The data gaps between days 120 and 230, and around day 320, 1987 are due to the sun angle restriction of the satellite. At the other times, we could monitor the source every few days.

4U 0115+63. Following our observation, H. Pedersen, S. Ilovaisky, and M. van der Klis (*IAU Circular* No. 4357, 1987) identified the optical counterpart of GS 1354−64. The bright X-ray nova GS 2000+25 was discovered on April 26, 1988, and its maximum intensity reached about 12 Crab (1–6 keV) (F. Makino and the Ginga team, *IAU Circular* Nos. 4588 and 4600, 1987). Following our discovery, the optical counterpart was identified (N. Okamura and T. Noguchi, *IAU Circular* No. 4589, 1988; R. M. Wegner, A. A. Henden and R. Bertram, *IAU Circular* No. 4600, 1988) and followed by the continuous monitoring of this source both in the X-ray and in the optical region. This source is strongly believed to include a black-hole candidate (Tsunemi et al. 1989).

3.2. *Historical Record (the Case of Cir X-1)*

Since we have six different fields of view, we can clearly distinguish an individual X-ray source even in the Galactic center region as shown in figure 5. In this way, we accumulate data from about one hundred galactic sources. These data will reveal their long-term variations on various time scales. For example, in figure 7 we show the light curve of Cir X-1 obtained by the ASM between February and December 1987 in the energy range 1–6 keV. On the vertical scale the value 1.8 corresponds to the intensity of the Crab Nebula. The data gaps between days 120 and 230, and around day 320, 1987 are due to the sun angle restriction of the satellite.

We searched the data for periodicity using the folding method and obtained the binary period of 16.58 ± 0.02 d with the maximum intensity occurring at JD = 2446854.36 ± 0.03. The maximum χ^2 from the constant intensity hypothesis is about 4200 with 9 degrees of freedom. In figure 8, we show the X-ray light curve of Cir X-1 folded modulo its orbital period. In this figure, the Crab Nebula intensity is 1.8 for the range 1–6 keV and 0.6 for 6–20 keV, respectively. Our data were obtained once every few days with an integration time of at most several seconds. Therefore, each datum does not always represent the mean intensity over a few days. The light curve we obtained shows a rapid increase on a time scale of about

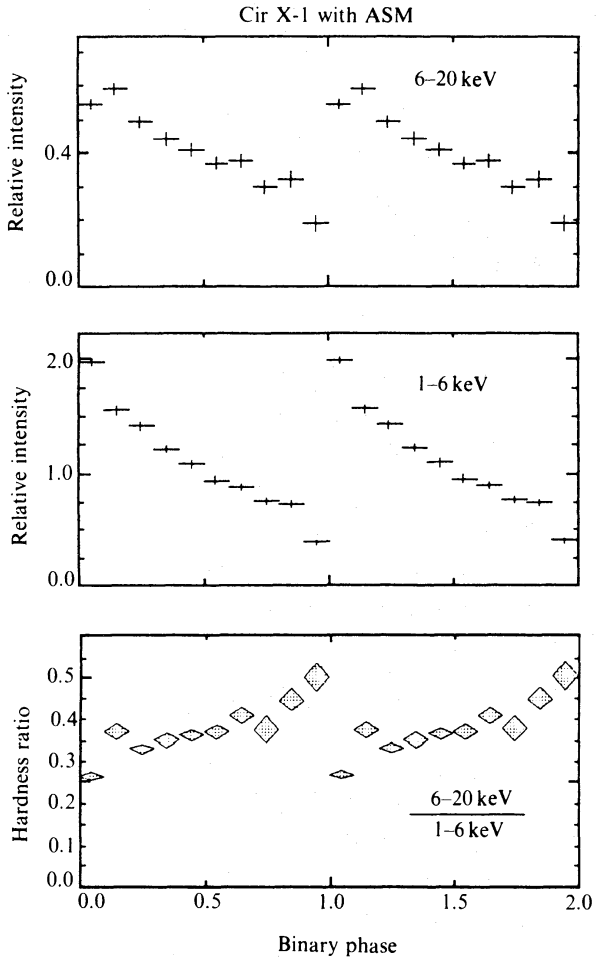

Fig. 8. The light curve of Cir X-1 is plotted over two periods folded modulo its binary cycle in the energy range of 6–20 keV (a) and 1–6 keV (b). The lower panel shows the hardness ratio: i.e. the ratio between (a) and (b). The Crab Nebula intensity is 1.8 for (a) and 0.6 for (b).

one day or less and a gradual decrease in its decay phase. So far, the exact time scale of the rapid increase is not well determined.

The binary period of Cir X-1 which we obtained is consistent with that reported by Kaluzienski et al. (1976), with Ariel V data, to within the statistical uncertainties. However, the folded light curve we obtained is quite different from theirs. The light curve in the period 1975 October and 1976 April showed a gradual increase followed by a rapid decrease with a time scale of less than 0.07 d. The light curve observed by Uhuru in 1972 (Forman and Jones 1976) showed a gradual increase as well as a gradual decrease. Subsequent observations by Copernicus (Davison and Tuohy 1975) and by COS-B (Bignami et al. 1977) showed the evolution of the light curve in the binary period. By contrast, the latest observation performed by Tennant (1987) revealed evidence for a rapid increase and a subsequent gradual decrease, although his observation did not cover the whole binary cycle. Our data clearly show a new aspect of the light curve of a complete binary cycle.

3.3. *Additional Results*

The ASM has a much wider field of view than that of the LAC on board the Ginga satellite. Since the ASM is in operation continuously, it can also observe some bright sources inside the field of view of the instrument when the satellite is in the pointing mode for LAC observations. During these periods, we can only obtain PC data with the time resolution of the data recorder (1/16–2 s). So far, we have observed several X-ray pulsars in this mode (F. Makino and Ginga team, *IAU Circular* No. 4459, 1987; Tsunemi 1989) including Vela X-1, Cen X-3, for example. We have found the longest pulse period of 283.09 ± 0.01 s for Vela X-1 and the shortest period of 4.8229 ± 0.0001 s for Cen X-3. In general, the ASM in the pointing mode is sensitive to X-ray pulsars whose apparent intensities are brighter than 10 mCrab (depending on the pulse fraction).

In addition, we wish to draw attention to the pointing observation of GS 2000+25 in its brightening phase (Tsunemi et al. 1989). We were fortunate to discover GS 2000+25, when it was at about 4% of its maximum brightness and be able to monitor it continuously for more than two days until its intensity was about 80% of its maximum.

4. Conclusions

Since launch, the ASM on board the Ginga satellite has been functioning as planned. It has covered about 70% of the celestial sphere in the normal slew 360 ASM mode. The detection limit is 50 mCrab or less in this observational mode. The ASM has achieved its objective as a real-time alarm for transient phenomena. It has also effectively monitored the galactic bright sources at least once every few days when they are within its accessible region, and has provided a historical record for archival investigation.

Furthermore, the ASM has obtained valuable data on X-ray sources even when the satellite is in the pointing mode for LAC observations. With these data, we have performed not only pulse timing analysis of X-ray pulsars but also monitored the activity of other X-ray sources which happened to be in the field of view. Finally, the ASM provides important historical archival records of X-ray sources which bridge those obtained by the previous experiments and the data to be obtained by future experiments.

The authors express their thanks to the other members of the Ginga team as well as the launching staff in the Institute of Space and Astronautical Science. They also thank Dr. J. Ling for providing many useful comments.

References

Bignami, G. F., Ventura, A. D., Maccagni, D., and Stiglitz, R. A. 1977, *Atron. Astrophys.*, **57**, 309.
Davison, P. J. N., and Tuohy, I. R. 1975, *Monthly Notices Roy. Astron. Soc.*, **173**, 33 P.
Forman, W., and Jones, C., 1976, *Bull. Amer. Astron. Soc.*, **8**, 541.
Holt, S. S. 1976, *Astrophys. Space Sci.*, **42**, 123.

Kaluzienski, L. J., Holt, S. S., Boldt, E. A., and Serlemitsos, P. J., 1976, *Astrophys. J. Letters*, **208**, L71.
Koyama, K., Ikegami, T., Inoue, H., Kawai, N., Makishima, K., Matsuoka, M., Mitsuda, K., Murakami, T., Ogawara, Y., Ohashi, T., Suzuki, K., Tanaka, Y., Waki, I., and Fenimore, E.E. 1984, *Publ. Astron. Soc. Japan*, **36**, 659.
Makino, F., and the ASTRO-C team 1987, *Astrophys. Letters Commun.*, **25**, 223.
Priedhorsky, W. C., Terrell, J., and Holt, S. S. 1983, *Astrophys. J.*, **270**, 233.
Tennant, A. F. 1987, *Monthly Notices Roy. Astron. Soc.*, **226**, 971.
Toor, A., and Seward, F. D., 1974, *Astron. J.*, **79**, 995.
Tsunemi, H. 1989, *Publ. Astron. Soc. Japan*, **41**, 453.
Tsunemi, H., and Kitamoto, S. 1988, *Astrophys. J. Letters*, **334**, L21.
Tsunemi, H., Kitamoto, S., Okamura, S., and Roussel-Dupré, D. 1989, *Astrophy. J. Letters*, **337**, L81.
Turner, M. J. L., Thomas, H. D., Patchett, B. E., Reading, D. H., Makishima, K., Ohashi, T., Dotani, T., Hayashida, K., Inoue, H., Kondo, H., Koyama, K., Mitsuda, K., Ogawara, Y., Takano, S., Awaki, H., Tawara, Y., and Nakamura, N. 1989, *Publ. Astron. Soc. Japan*, **41**, 345.